Nonlinear Characterization of a Joint Exhibiting a Reduction in Damping at High Energy

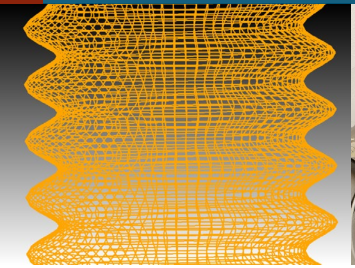

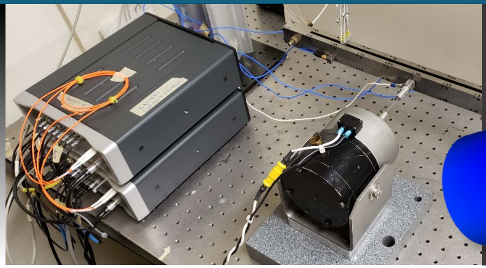

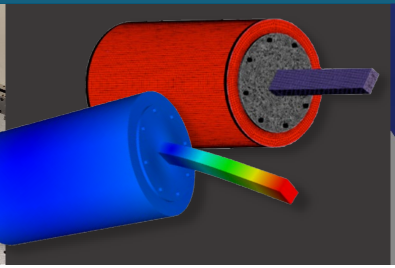

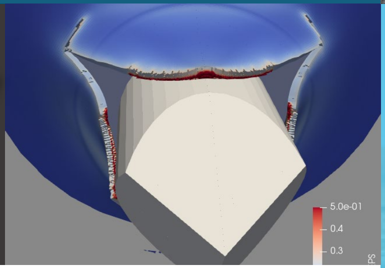

STUDENTS

Daniel Agramonte, Gabrielle Graves, Kenneth Meyer

MENTORS

Ben Pacini, Matt Allen, Mo Khan, David Najera, Dan Roettgen

SAND2021-8886 PE

Sandia National Laboratories is a multimission laboratory managed and operated by National Technology & Engineering Solutions of Sandia, LLC, a wholly owned subsidiary of Honeywell International Inc., for the U.S. Department of Energy's National Nuclear Security Administration under contract DE-NA0003525.

Meet the Interns!

Fig 0a. Daniel Agramonte
University of Georgia

Fig 0b. Gabrielle Graves
New Mexico State University

Fig 0c. Kenneth Meyer
University of Texas at Austin

Background And Motivation – Previous Experiment

- During tension/compression fatigue testing of the bolt connecting a kettlebell to a fixture, a decrease in damping was observed with increased excitation amplitude.
- Damping generally increases as excitation amplitude increases – this was unexpected

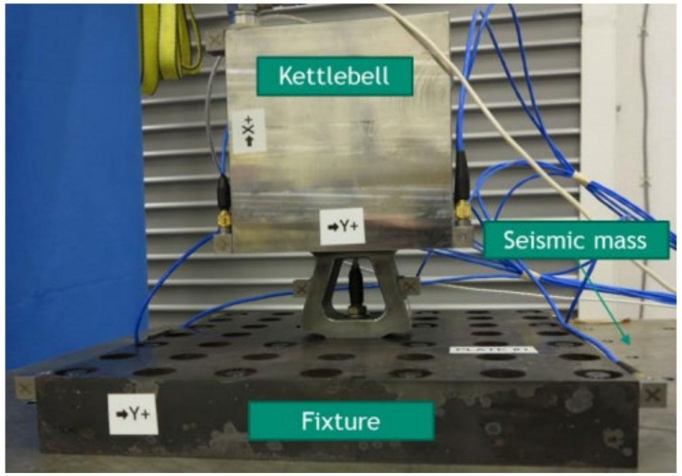

Fig 1. Test setup

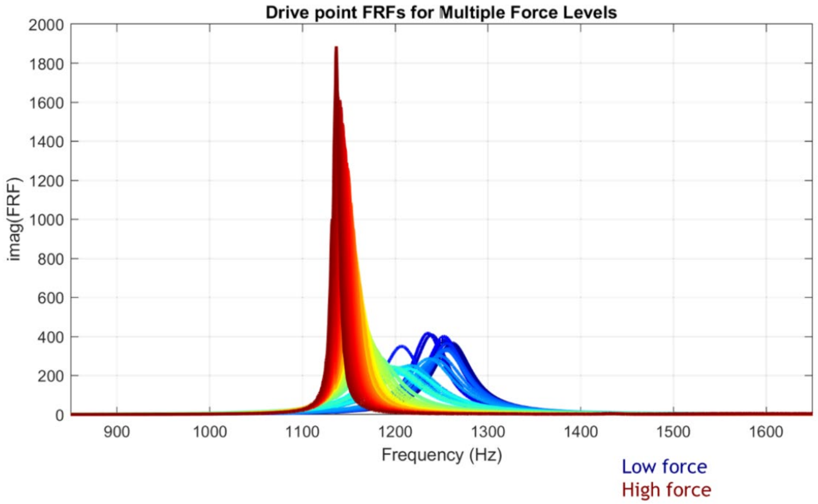

Fig 2. FRFs for various forcing levels

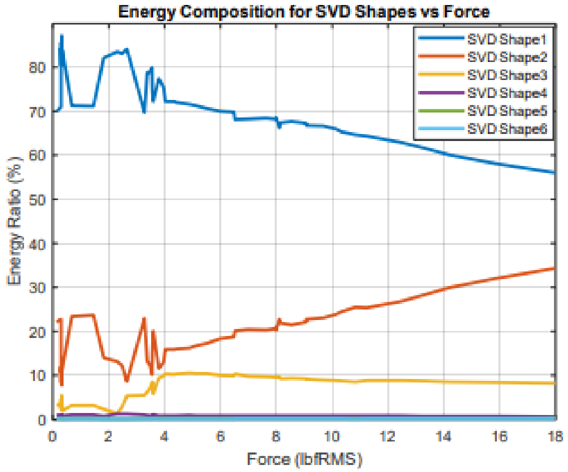

Fig 3. SVD Shapes

- Motivating question: is the decrease in damping due to modal coupling, or a nonlinear characteristic of one of the modes in question (the 2^{nd} bending mode in Y (4), and the axial mode in X (5))?
- The SVD shapes in figure 3 represent the modal deflection shapes and is derived from the columns of the FRF matrix
  - Presence of 2 modes indicates that coupling could be occurring

Objectives

Project Goal: Determine if the decrease in damping is caused by modal coupling of the axial and 2^{nd} bending mode in Y

Tasks:

1. Perform linear modal and nonlinear testing
   - Nonlinear identification of the axial and 2^{nd} bending mode in Y
2. Create nonlinear finite element model
3. Create a nonlinear Hurty-Craig-Bampton (HCB) reduced order model
   - Capture nonlinearities with Iwan elements
4. Conduct MM-QSMA on the full fidelity finite element model
   - QSMA has only been used to examine weakly coupled structures

Experimental Setup

- Kettlebell-plate system is similar to the setup used for tension/compression failure testing
- 4340 Steel Kettlebell
- Boundary Conditions: Fixed base – Free end

Location of Hammer Impacts

- Node 1001 excites axial mode (mode 4)
- Node 1002 excites both modes
- Node 1003 excites 2nd bending mode (mode 5)

Fig 4. Close-up of contact between the kettlebell and plate

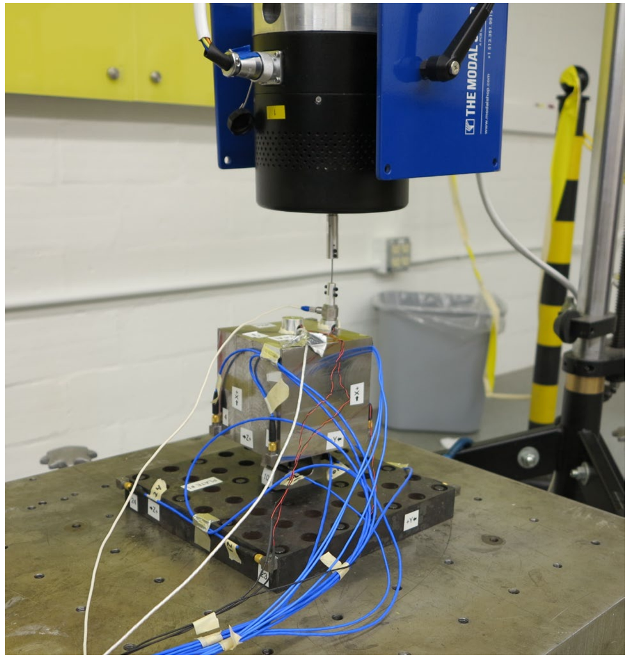

Fig 5. Full setup for a shaker test

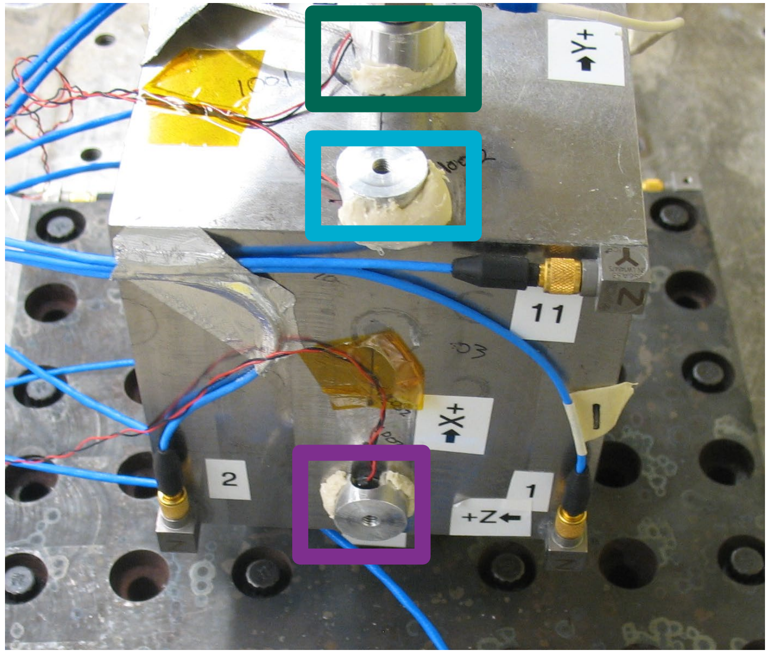

Fig 6. Close-up of kettlebell with reference node/drive point locations

Structure Rotation

- The Kettlebell-Fixture structure rotated slightly in the z direction a Force Appropriation test!
- Linear natural frequency and damping shifted in each mode as a result

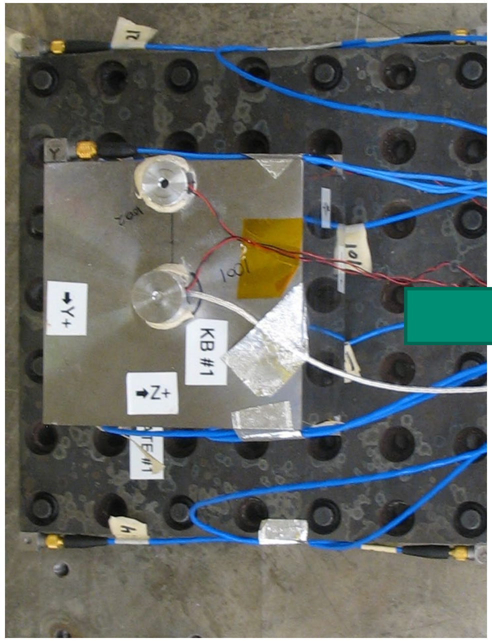

Fig 7. Original Structure

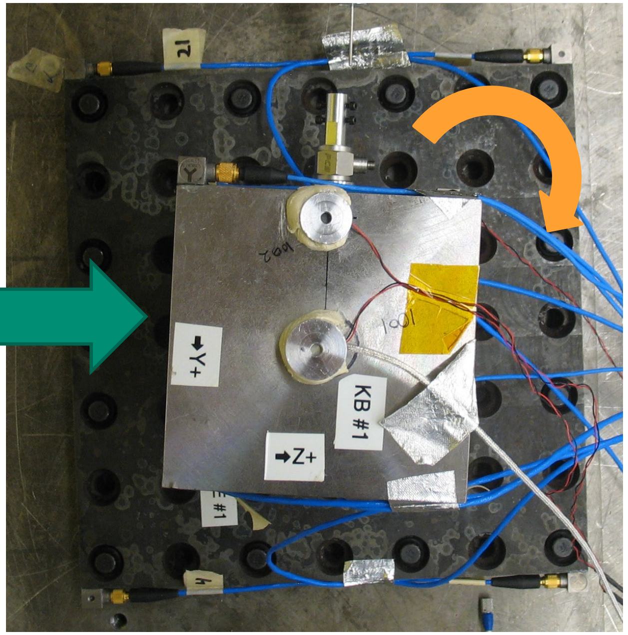

Fig 8. Rotated Structure

Table 1. Frequency Shift

Mode	$f_n\ (Hz)$	$f_{n-rot}\ (Hz)$	*Change*
1st Bending in Z	84.9	101.5	19.55%
1st Bending in Y	166.8	178.9	7.25%
Torsion about X	328.7	348.1	5.90%
2nd Bending in Y	1132.1	1137.3	0.46%
Axial in X	1145.4	1182.3	3.22%
2nd Bending in Z	1429.6	1469.0	2.76%

- Separation between axial and bending modes increased!
  - Previously separated by ~13 Hz, now separated by 45 Hz

Governing Equations and Linearized Results

- We model the physical system using a system of equations

$$M\ddot{x} + C\dot{x} + Kx = f \quad \text{Eqn. 1}$$

$$\ddot{q} + 2\zeta_n \omega_n \dot{q} + \omega_n^2 q = \phi^t f \quad \text{Eqn. 2}$$

- Given an excitation force f and known natural frequencies and damping ω_n and ζ_n, we can solve for the modal and physical response of the system, q and x
- Extraction of modes for low-level input data – response is effectively linear at low force levels
- Bending and Axial modes are fit well with the extraction
- Equation for FRF (Frequency Response Function) used to extract the mode shapes:

$$H_{ij}(\omega) = \sum \frac{-\omega^2 \phi_{ik} \phi_{jk}}{\omega_k^2 - \omega^2 + i2\zeta_k \omega \omega_k} \quad \text{Eqn. 3}$$

- Each column of the FRF matrix (H) corresponds to the individual FRF for each mode

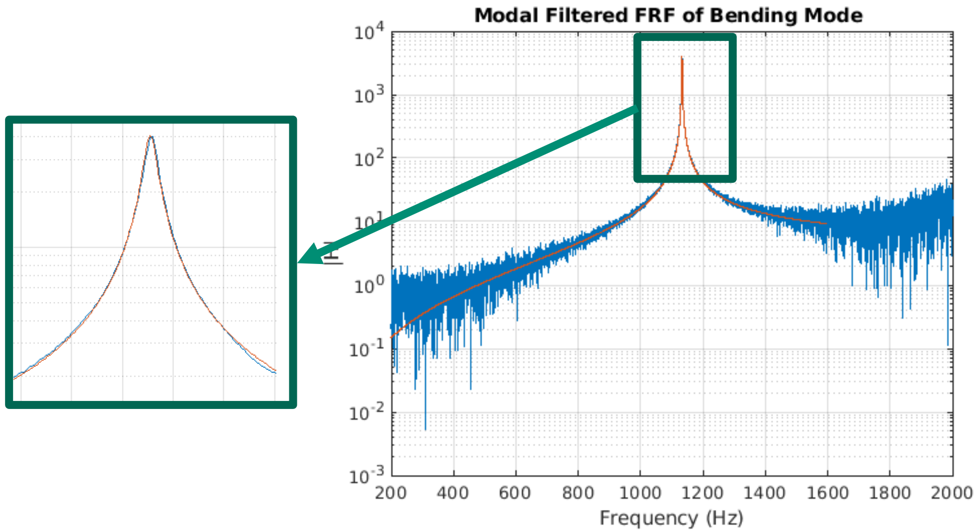

Fig 9. Bending Mode Extraction

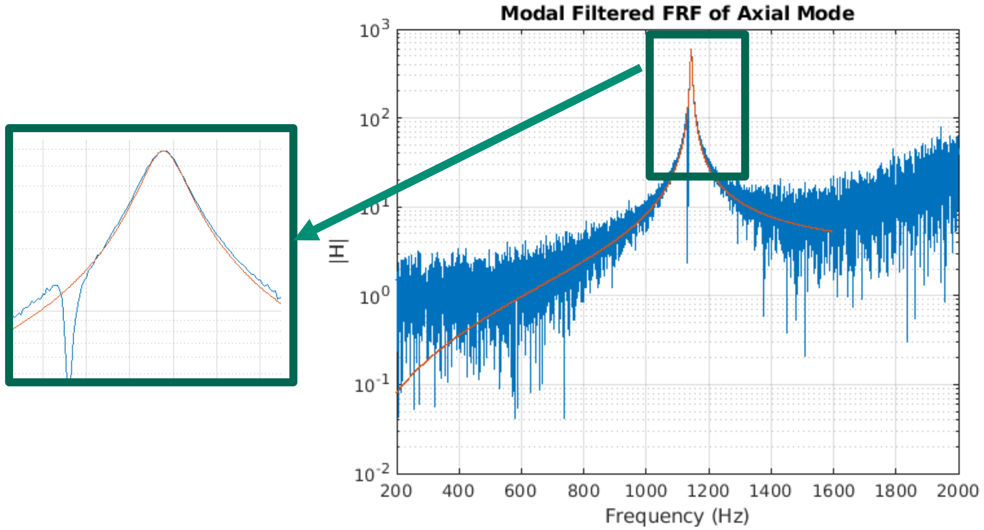

Fig 10. Axial Mode Extraction

Nonlinear Identification

- Using acceleration data and known mode shapes, we can compute the nonlinear natural frequency and damping of the structure (flow chart from Ben Pacini)

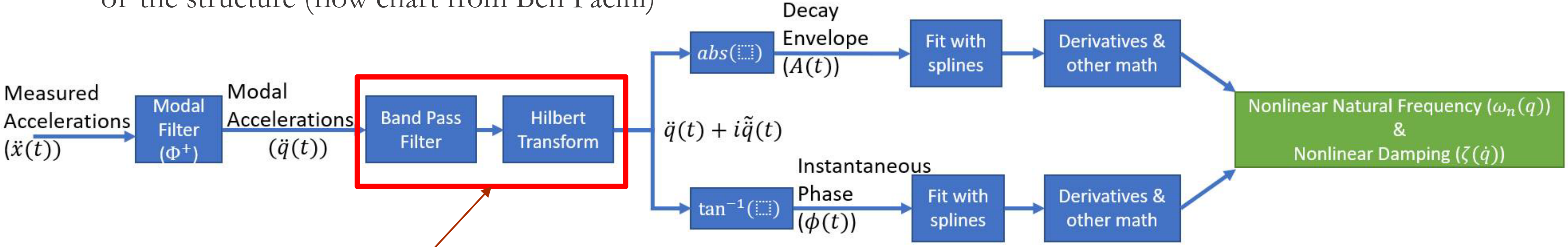

Fig 11. Nonlinear Amplitude Dependent Natural Frequency and Damping Workflow

- Standard Hilbert Transform did not filter the bending and axial modes well due to closeness of modes
- Other filters (Butterworth and Chebyshev2) and transformation methods (Short Time Fourier Transform) were attempted, but also do not properly filter response
- A new method must be used – nonlinear optimization is used to curve fit the oscillation
  - This method was discovered too late in NOMAD 2021 to be properly used/implemented in the reduced order modeling of the system
  - $\tilde{y}(t) = e^{\beta(t)} \cos(\alpha(t))$ (Ben Moldenhauer)

Picking the Right Band-Pass filter

- Shoulder due to bending mode appears in FRF of axial mode
- Narrow filters do not properly model response of axial mode – peak acceleration is not the same
- Thus, we need an alternative method to filter the data

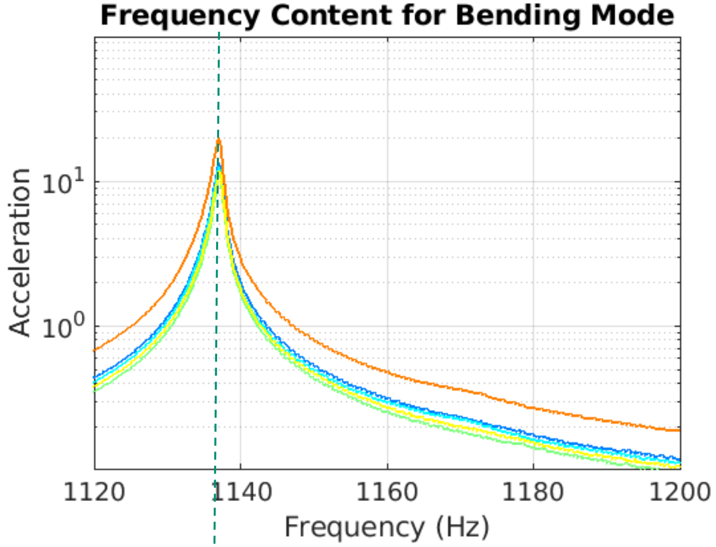

Fig 12a. FRFs for Bending mode

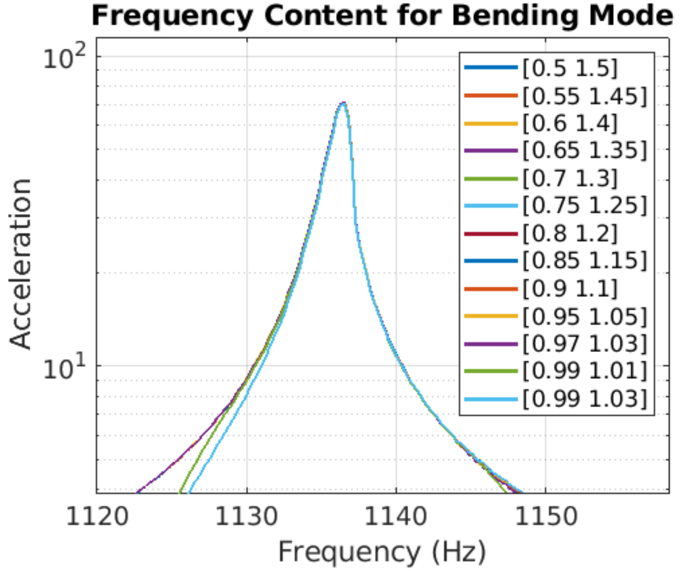

Fig 12a. FRFs for various bandpass filters

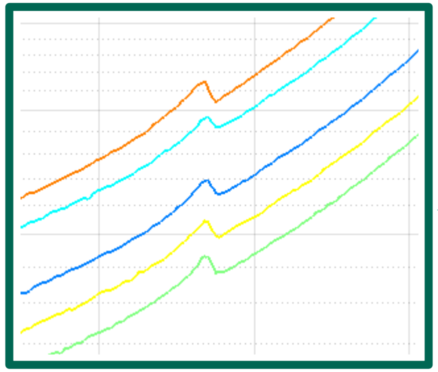

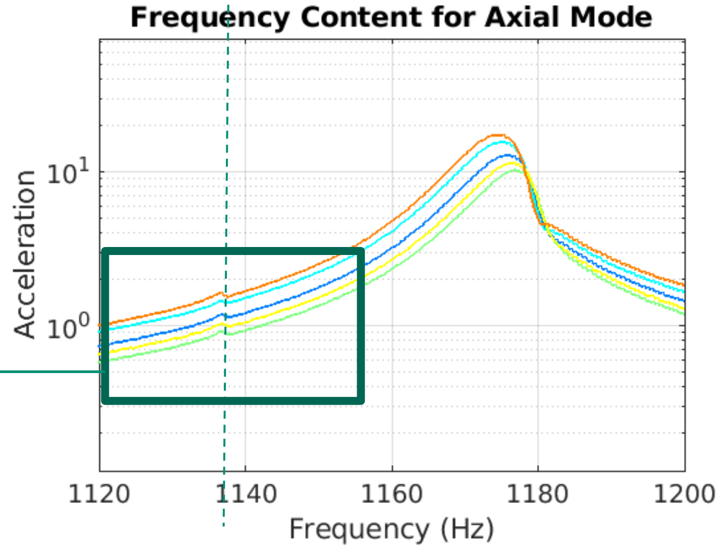

Fig 13b. FRFs for Bending mode

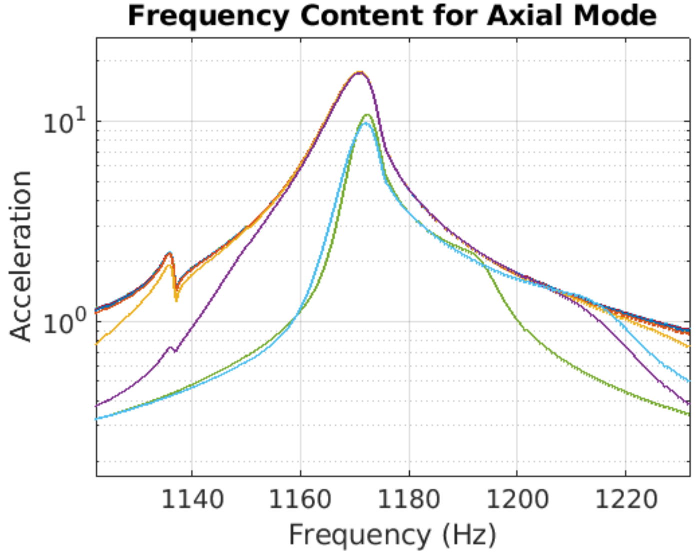

Fig 13b. Roll-off Effects of Different filters

Structure Rotation – New Frequency And Damping

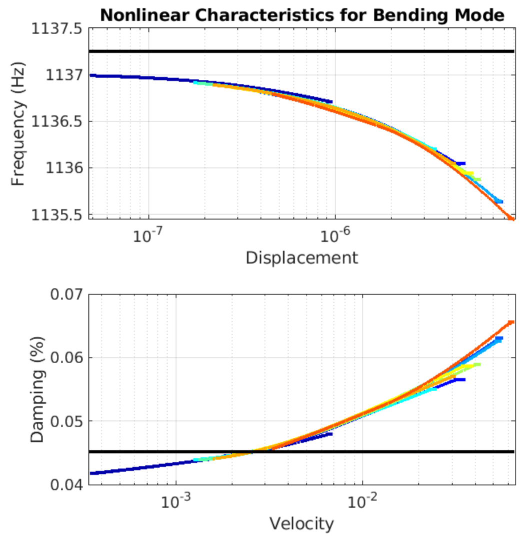

Fig 14a. Individual ω_n and ζ_n - bending

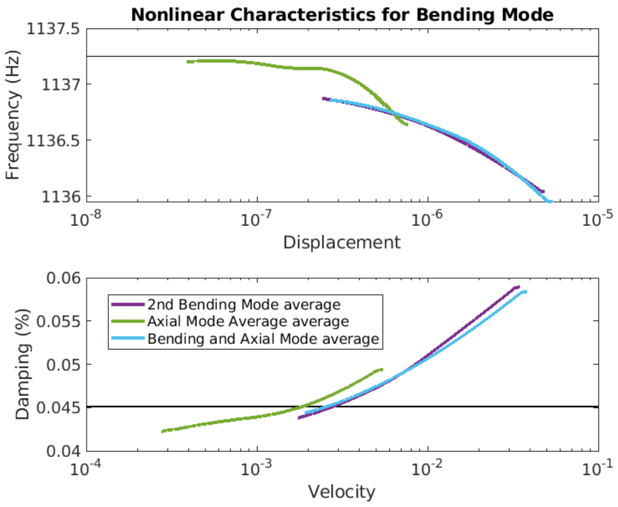

Fig 14b. Averaged ω_n and ζ_n - bending

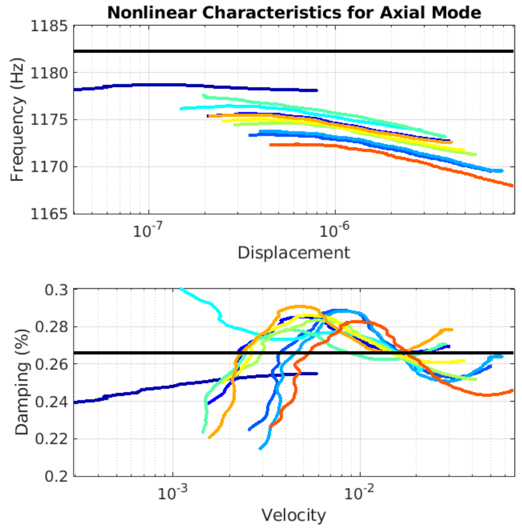

Fig 14c. Individual ω_n and ζ_n - axial

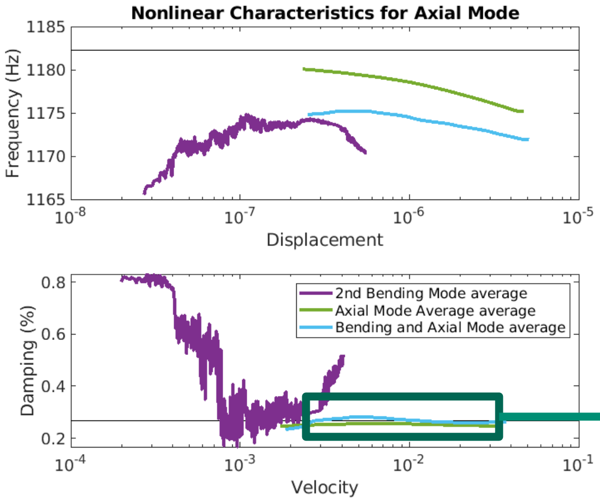

Fig 14d. Averaged ω_n and ζ_n - axial

- Isolated axial mode damping curve is concave down; previously concave up
- Behavior of bending mode is constant during isolation and joint excitation with axial mode
  - This indicates that there is less coupling occurring between the axial and bending modes
- Axial mode is non-monotonic
  - This presents problems with using an Iwan spring for the nonlinear model

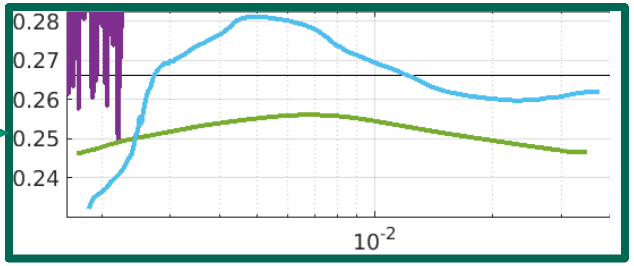

Quasi Static Modal Analysis (QSMA)

- Determines the quasi-static response of a structure when a force in the shape of a mode of interest is applied
  - Determines nonlinear natural frequencies and damping ratios (amplitude dependent)
  - Allows modes shapes to change with amplitude
  - Not conventionally used to determine modal coupling
  - Modal coupling can be assessed by the skew of each mode when only one mode is meant to be activated

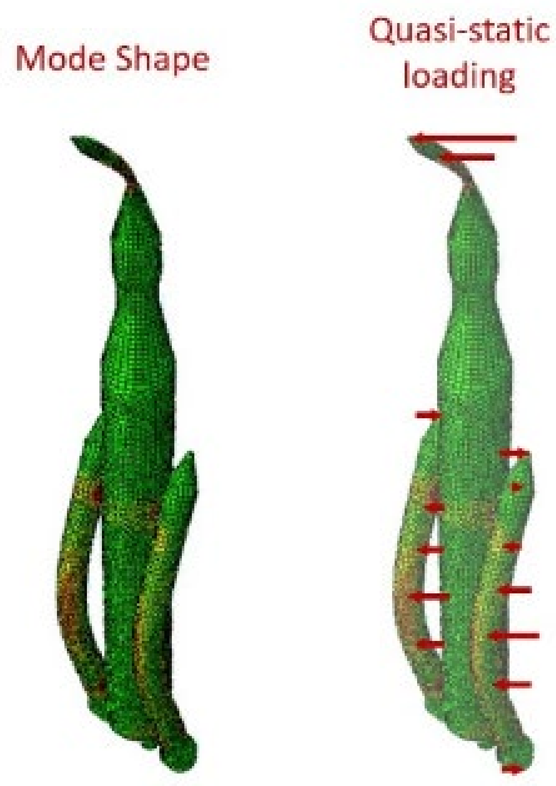

$$\mathbf{f}_{ext} = \mathbf{M}\,\boldsymbol{\phi}_r$$

$$\underbrace{\omega_r(\alpha) = \sqrt{\frac{\alpha}{q_r(\alpha)}}}_{\text{Amplitude dependent frequency}} \quad \text{Eqn. 4}$$

$$\underbrace{\zeta_r(\alpha) = \frac{D(\alpha)}{2\pi(q_r(\alpha)\omega_r(\alpha))^2}}_{\text{Nonlinear Damping}} \quad \text{Eqn. 5}$$

Nonlinear FEM: Linearized Modes

- High fidelity of model of Kettlebell structure with nonlinear joint interface contact to examine linear modes of vibration
  - Bolt is vital part of QSMA so the nonlinearities of joint can be assessed
  - 163173 tetrahedral elements
  - Bolt preload: 2025 lbf

Table 2. Linear Mode Preliminary Data

Mode	Model	Experimental	Error
1st Bending in Z	124.21	101.5	23%
1st Bending in Y	186.48	178.9	4.2%
Torsion about X	383.35	348.1	10%
2nd Bending in Y	1143.9	1137.3	0.6%
Axial in X	1255.2	1182.3	6.15%
2nd Bending in Z	1542.6	1469.0	5%

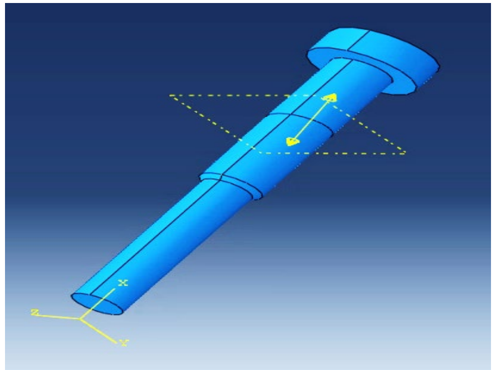

Fig 15. Bolt

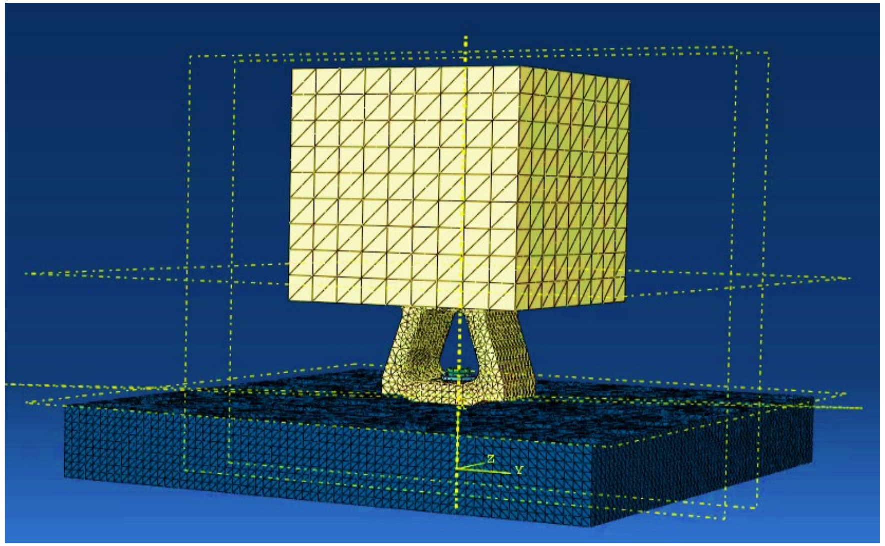

Fig 16. Pic of Model

Nonlinear FEM: Mode Shapes & Modal Assurance Criterion

- Correlates the simulated mode shapes with the experimental mode shapes.
  - > 90%, simulated has good agreement with experimental
  - Modes 1-6 have the appropriate correlation between exp. and sim.
  - Experimental mode shape data is collected form 11 tri-axial accelerometers

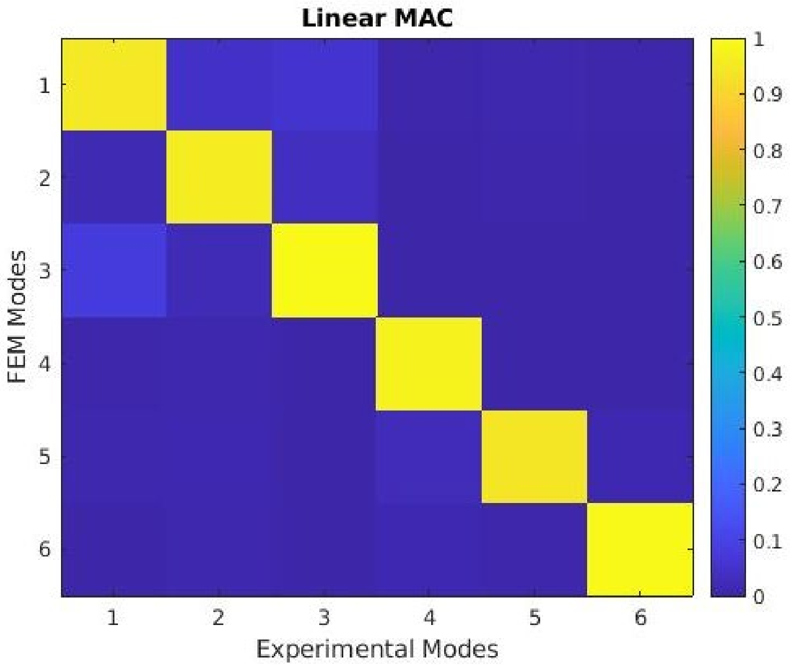

Fig 17. MAC

$$MAC(r,q) = \frac{\left|\{\varphi_A\}_r^T \{\varphi_X\}_q\right|^2}{\left(\{\varphi_A\}_r^T \{\varphi_A\}_r\right)\left(\{\varphi_X\}_q^T \{\varphi_X\}_q\right)}$$

Eqn. 6

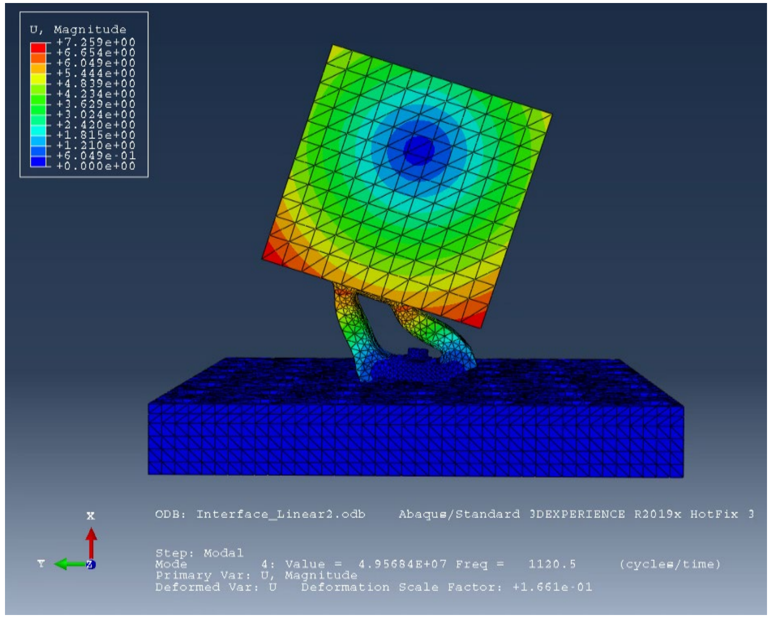

Fig 18. Pic of 2nd Y Bending mode

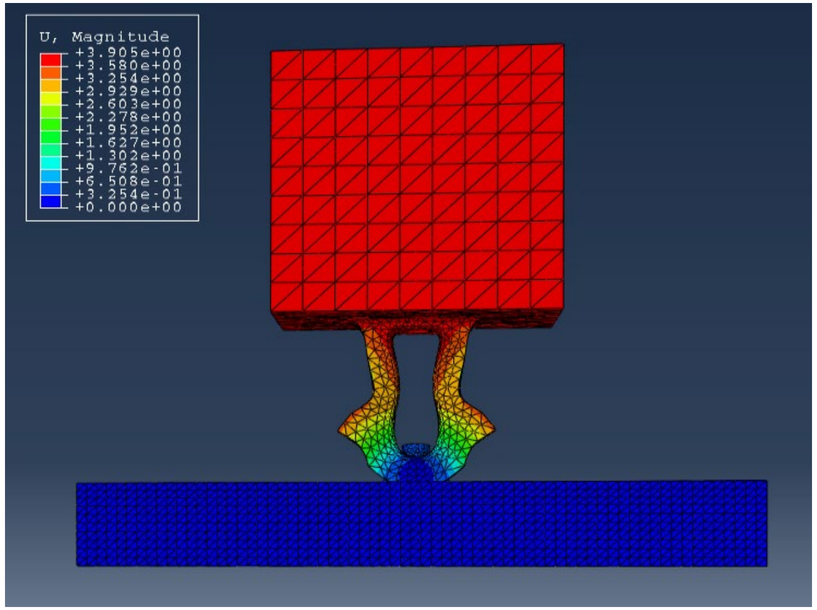

Fig 19. Pic of axial mode

Axial & Bending-Y Mode Results

- The Axial mode damping ratio monotonically
  - Inconsistent with FRF plot, show initial increase in damping followed by sudden decrease
  - The initial QSMA-derived natural frequency has a 2% error from experimental results
- The 2nd bending in y mode shows hardening effect and a increase in the damping ratio
  - Damping ratio behaves monotonically
- Results are inconsistent with the experimental results

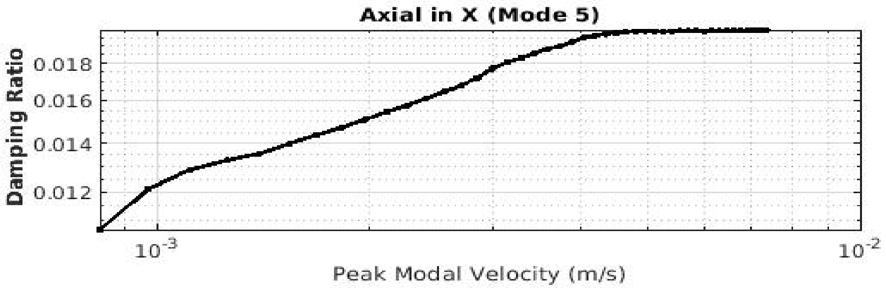

Fig 20. Axial Mode amplitude dependent data

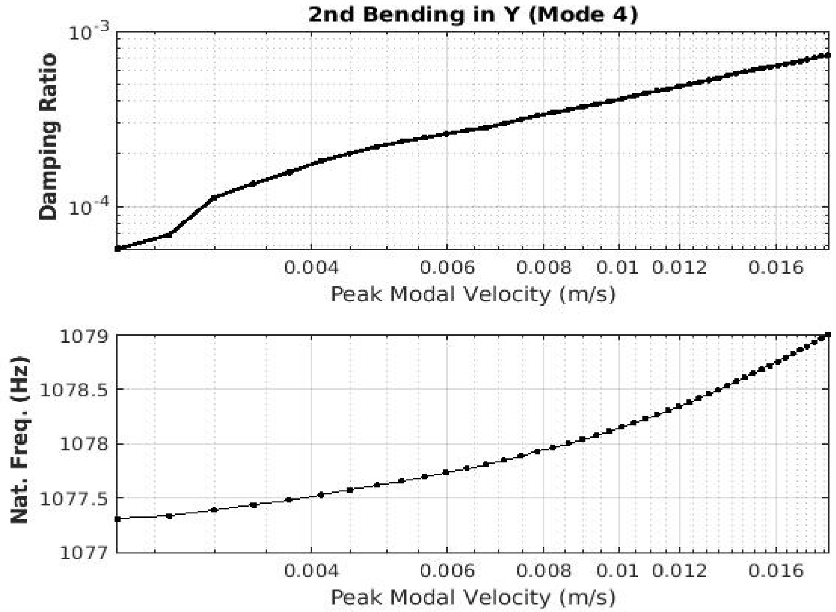

Fig 21. Bending in Y amplitude dependent data

Interface Static Analysis: Axial & 2^{nd} *Y bending mode*

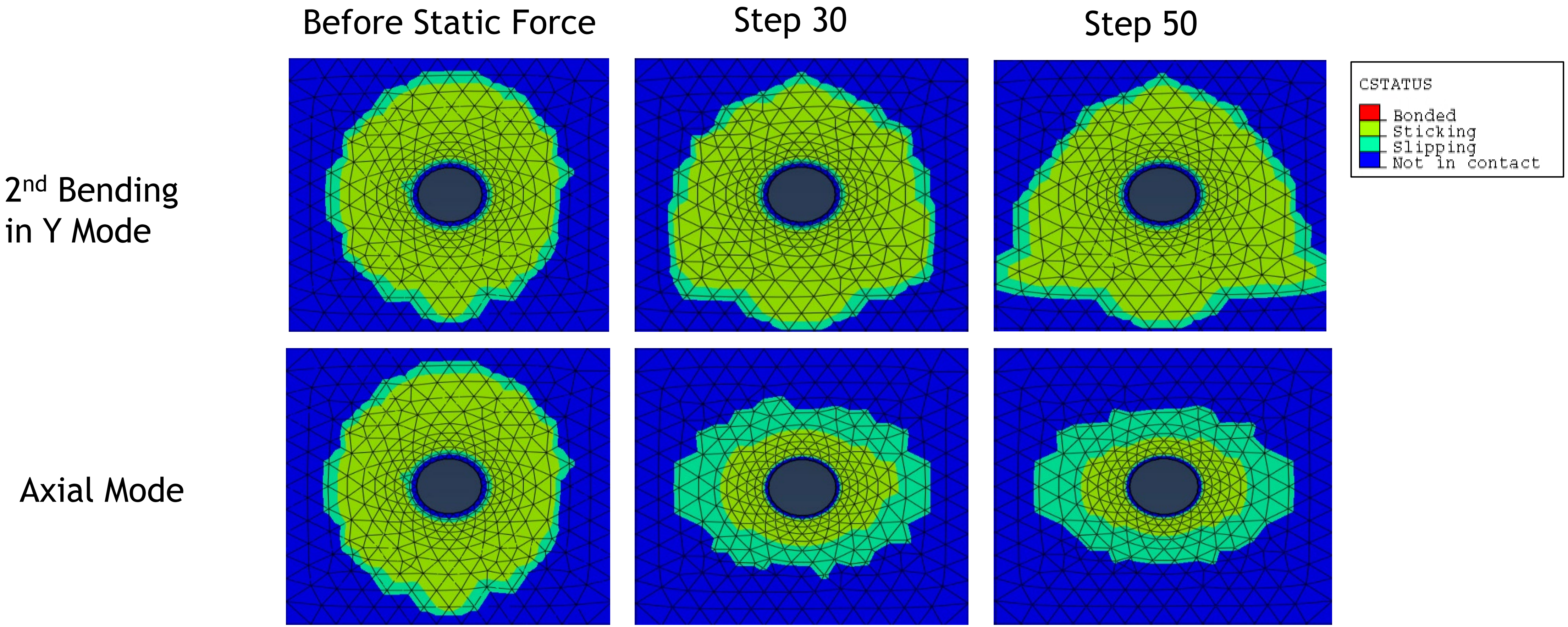

Fig 22a-f. Pressure distribution and Slip-Stick conditions (rep)

- 2^{nd} bending in Y slipping region remains around edges of stick region while stick region is increasing with amplitude
  - This causes increase of stiffness as amplitude increases (nonlinear hardening)
- Axial mode slip region decreases and slip region increases causing decrease in stiffness (nonlinear softening)

Nonlinear FEM: QSMA Results

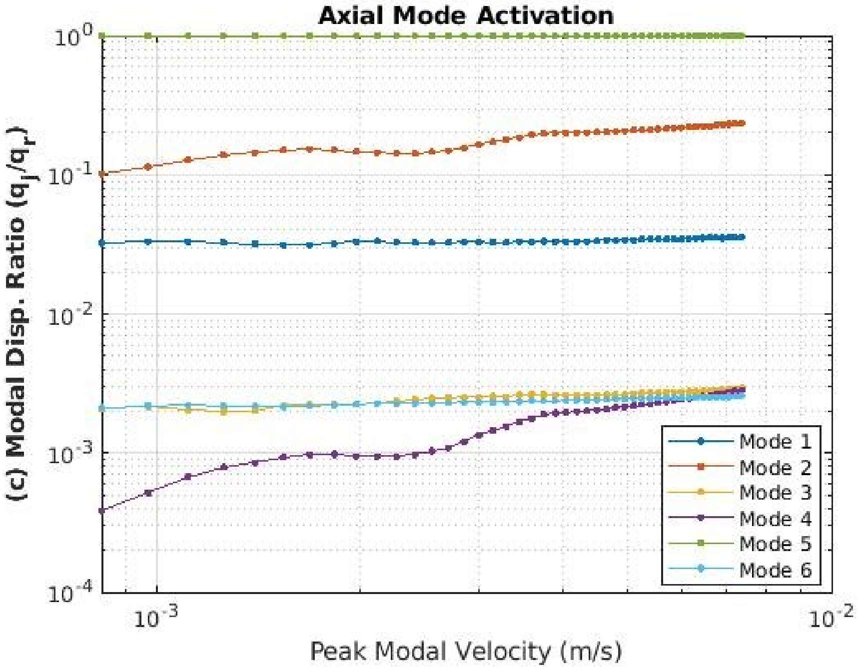

Fig 23. Modal coupling w/ axial as mode of interest

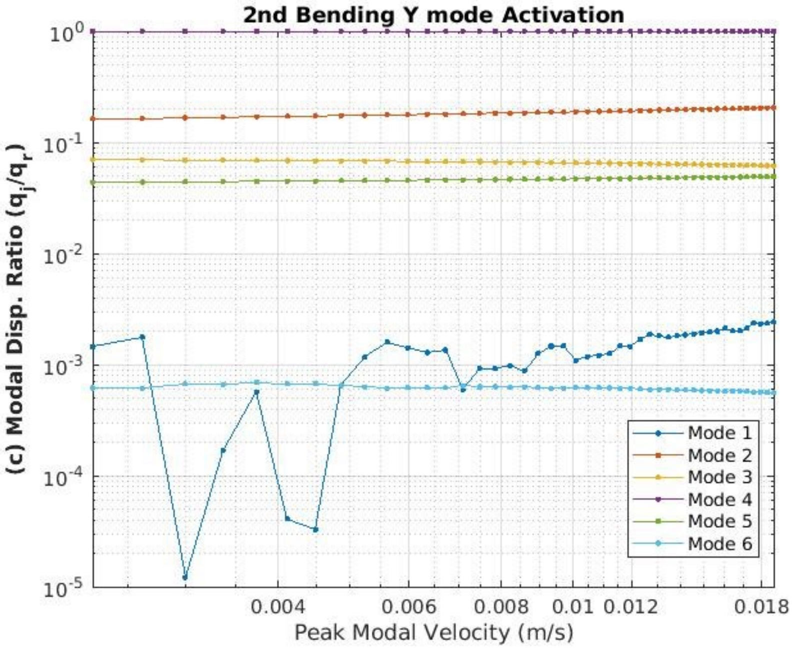

Fig 24. Modal coupling w/ bending- y as mode of interest

- Displacement of modes at amplitudes indicates activation and coupling
- Axial mode has considerable coupling with mode 1st bending mode in y
- 2nd bending mode in Y has considerable coupling with modes 1st bending in Y, Torsional mode in X, and Axial mode in X

Contact Interface Determination

- The contact interface between the adaptor plate and kettlebell was determined using Mo Khan's Sierra/SM simulation with a bolt preload of 2000lbf
- From this simulation, the contact patch size was estimated to be a circle with a diameter of 1.1"

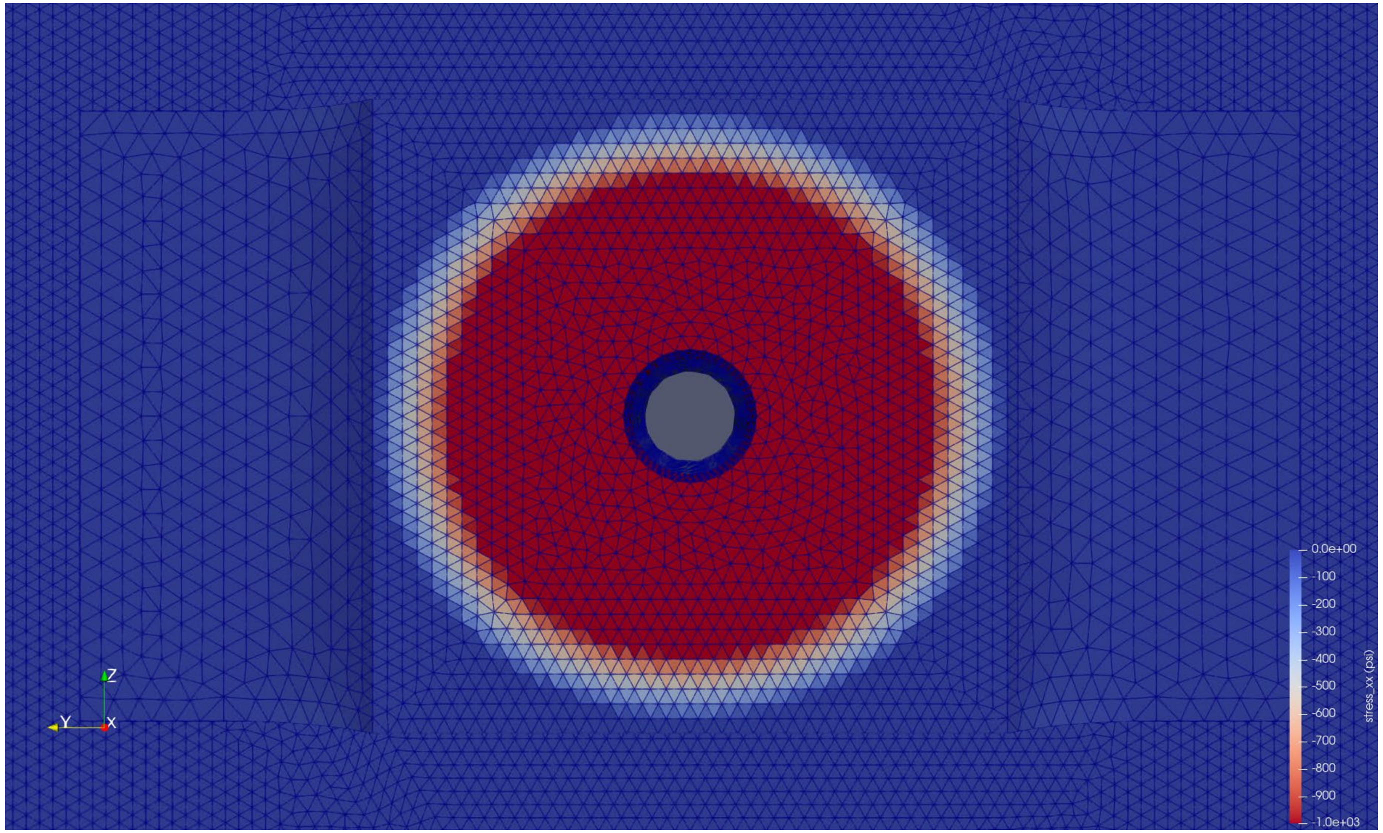

Fig 25. Contact Interface Pressure Distribution

Mesh Generation within Cubit

- Mesh was generated within Cubit with 923,662 nodes
- Mesh only failed the general guideline for the Scaled Jacobian on 3 elements, and given the size of the model, this level of failure was deemed acceptable

Table 4. Mesh Quality Summary

Function Name	Average	Standard Deviation	Minimum	Maximum	General Guideline
Shape	0.8508	0.077	0.4293	0.9996	>0.4
Normalized In-radius	0.7735	0.1026	0.2219	0.9985	>0.2
Scaled Jacobian	0.6471	0.1221	0.1846	0.9951	>0.2
Aspect Ratio	1.239	0.1594	1.000	3.467	<4.000

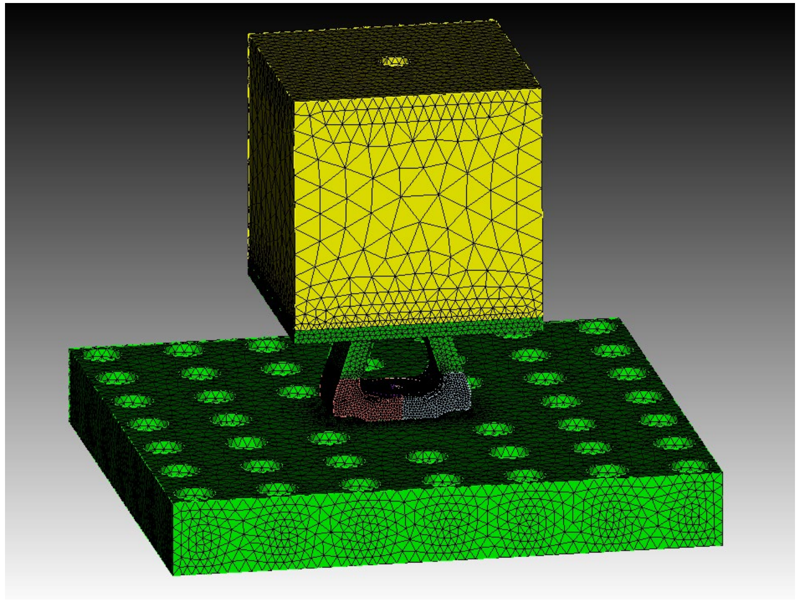

Fig 26. Kettlebell Meshed Geometry

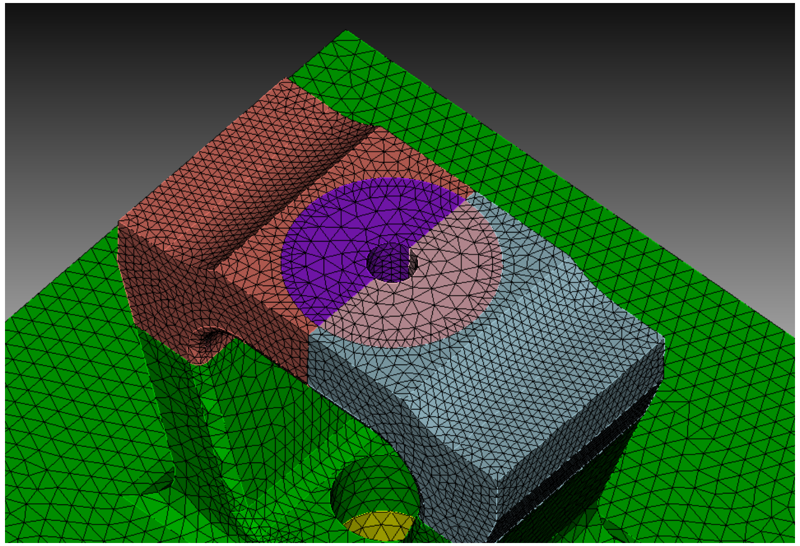

Fig 27. Contact Interface Mesh

Dynamic Sub-structuring with the HCB Approach

- The model was dynamically sub-structured into two super-elements: the adaptor plate and the kettlebell
- This was done to focus the analysis on the joint between the two parts
- Joint is initially modeled as a spring with stiffness in all 6 DOF's (3 linear + 3 rotational) with RBAR links tying contact nodes to a single interface node
- Computation speed was decreased by a factor of ≈54,000 and model size was reduced to 72 DOF's

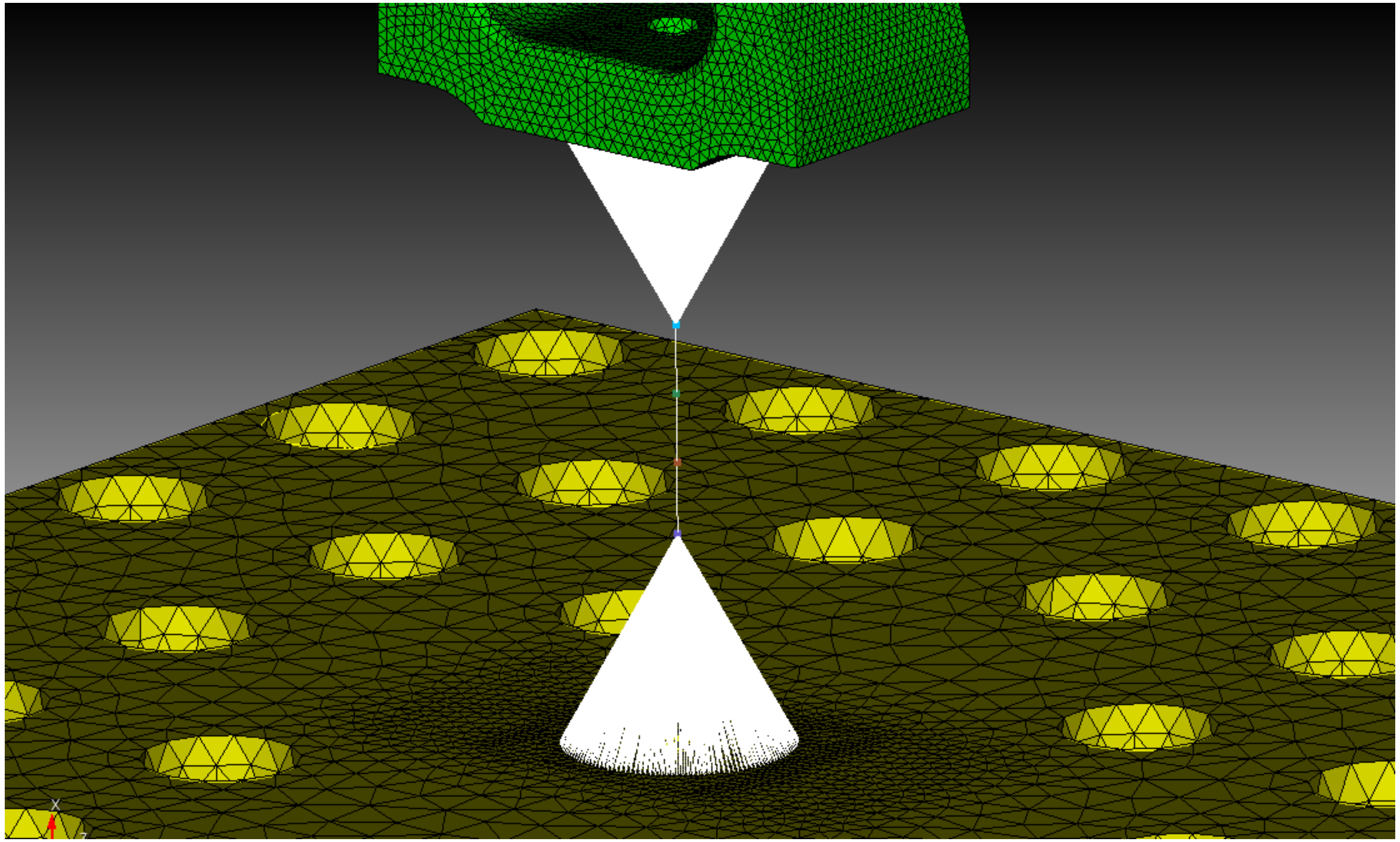

Fig 28. Contact Interface Modelling Approach

Linear Model Updating

- An inverse problem was formulated and solved by Sandia's Rapid Optimization Library (ROL) in order to tune the HCB model with experimental natural frequency truth data
- Poor fit of experimental axial mode due to slight bending in y-direction

Table 5. Linear Model Updating in Sierra

Mode	*Model*	*Experimental (Truth)*	*Error*
1st Bending in Z	101.614	101.5	0.112%
1st Bending in Y	178.890	178.9	0.006%
Torsion about X	348.076	348.1	0.007%
2nd Bending in Y	1137.250	1137.3	0.004%
Axial in X	1182.250	1182.3	0.004%
2nd Bending in Z	1458.200	1469.0	0.735%

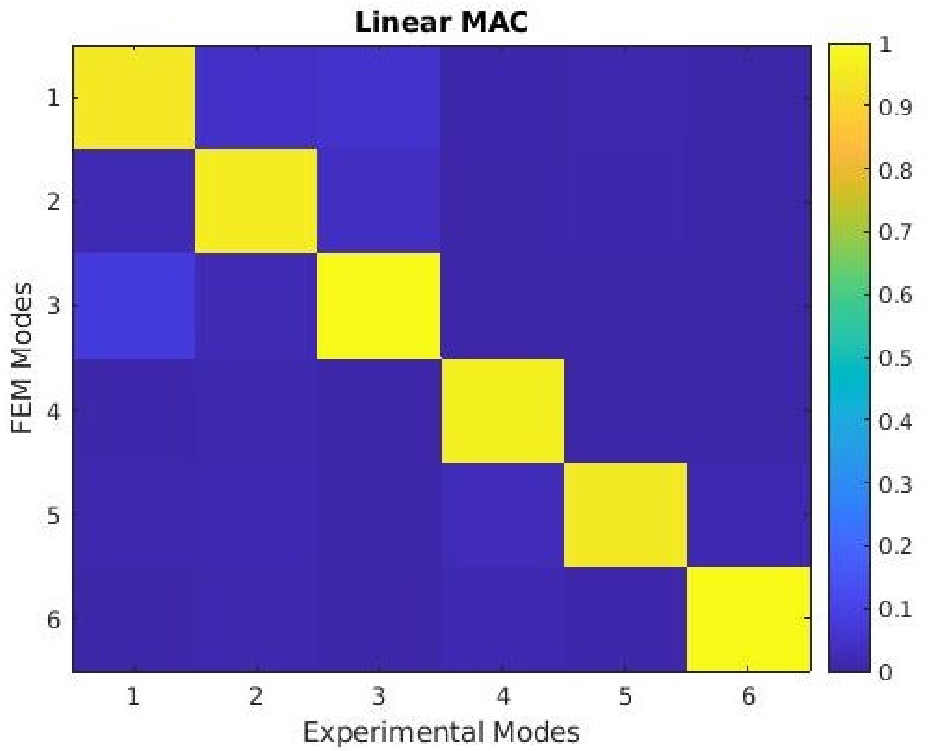

Fig 29. MAC for Linear Model

Iwan Spring Theory

- An Iwan spring consists of multiple Jenkins sliders (i.e., frictional sliders with springs) attached in parallel
- A typical hysteretic cycle for an Iwan spring is shown below

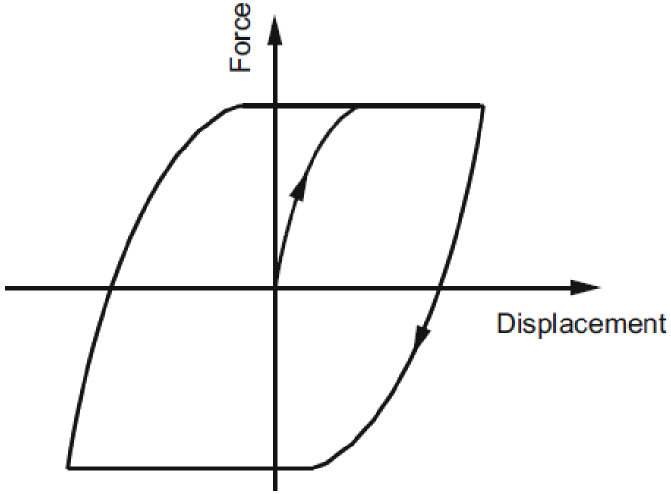

Fig 30. Iwan Spring Hysteretic Cycle

$$F_{IWAN} = \frac{F_S(\chi+1)}{\phi_{MAX}^{\chi+2}\left(\beta+\frac{\chi+1}{\chi+2}\right)}\left(\left(\frac{1}{\chi+2}-\frac{1}{\chi+1}\right)u^{\chi+2}+\frac{\phi_{MAX}^{\chi+1}}{\chi+1}u\right)+\frac{F_s}{\phi_{MAX}}\frac{\beta}{\beta+\frac{\chi+1}{\chi+2}}\Gamma(u,\phi_{MAX}) \quad \text{Eqn. 11}$$

$$\Gamma(u,\phi) = \begin{cases} u & u < \phi \\ \phi & u \geq \phi \end{cases} \quad \text{Eqn. 12}$$

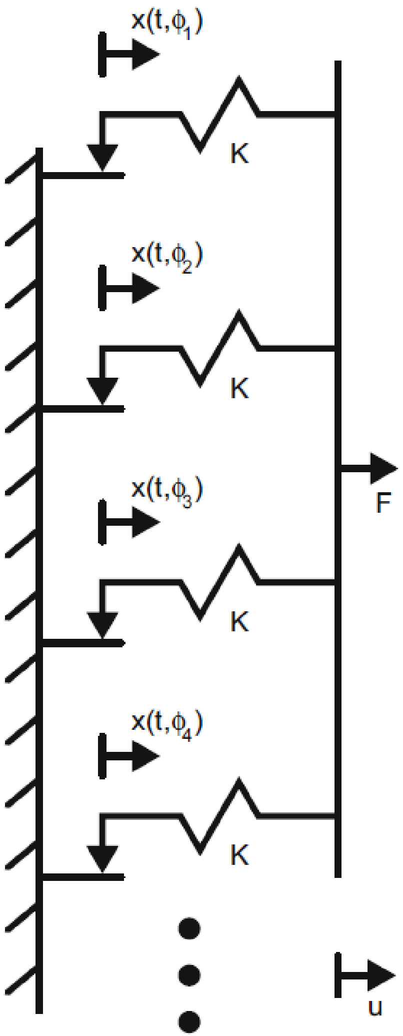

Fig 31. Iwan Spring Schematic

Nonlinear Model Formulation

- The frequencies of the 2nd bending mode in Y and the axial mode are highly dependent on the joint stiffness in the rot-Z and linear-X directions, respectively
- Iwan joints were placed in these directions to simulate slipping in these directions

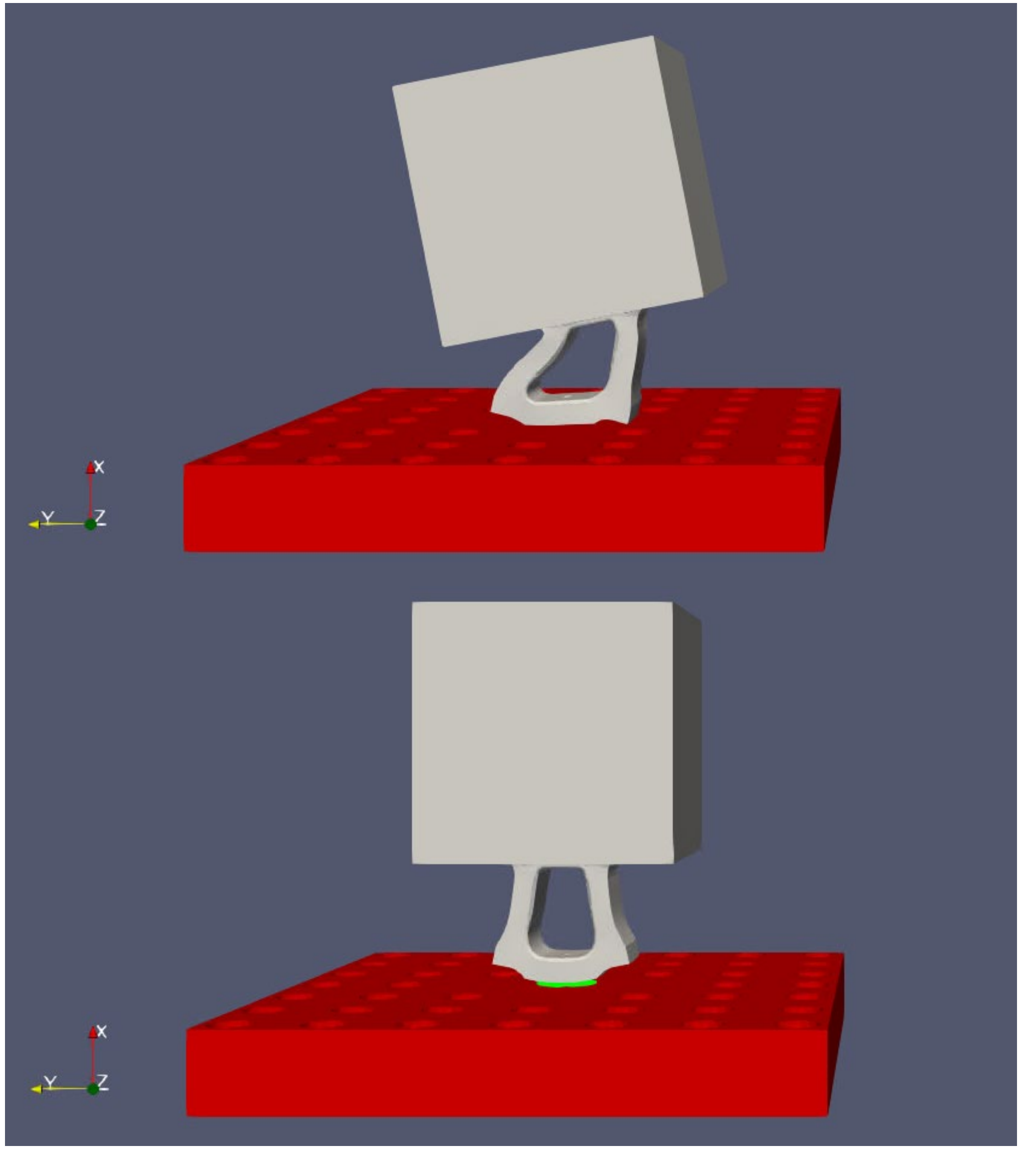

Fig 32a-b. Axial and 2nd bending in Y mode shapes

Nonlinear Model Updating

- A nonlinear optimizer was used to tune Iwan parameters within MATLAB
- Poor agreement with damping of axial mode
  - Physics of systems cannot be captured by Iwan spring

Table 6. Tuned Iwan Parameters

	F_s	$\gamma \cdot K_T$	χ	β
Linear-X	0.004889 lbf	26672231 lb/in	0.1858	3.4742
Rot-Z	3.2581e-5 lbf	12485674 lb/in	0.2194	0.01434

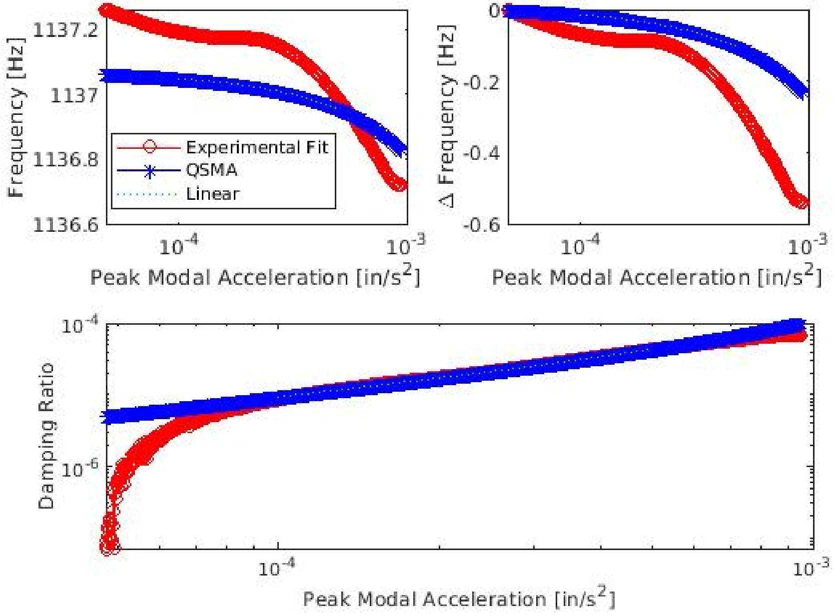

Fig 33. Iwan Spring Tuning for Second Bending Mode

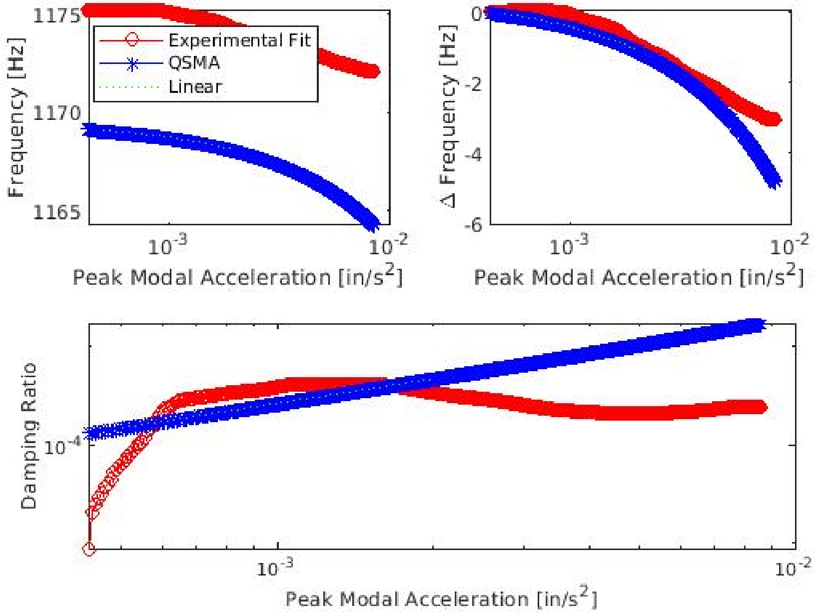

Fig 34. Iwan Spring Tuning for Axial Mode

Potential Constitutive Model and Physical Mechanisms

- A number of physical mechanisms and models have been proposed to explain the behavior of the joint in question:
  1. Constitutive model which assumes linear damping of joint but nonlinear stiffness dependent on integral average of linear stiffness at a given bolt force and loading amplitude
     - Affect of reduced contact area on material damping
  2. Modal coupling through Poisson's effect
  3. Multiple Asperity Contact
  4. Asymmetry of contact pressure distribution
  5. Mix of the aforementioned effects (1-4)

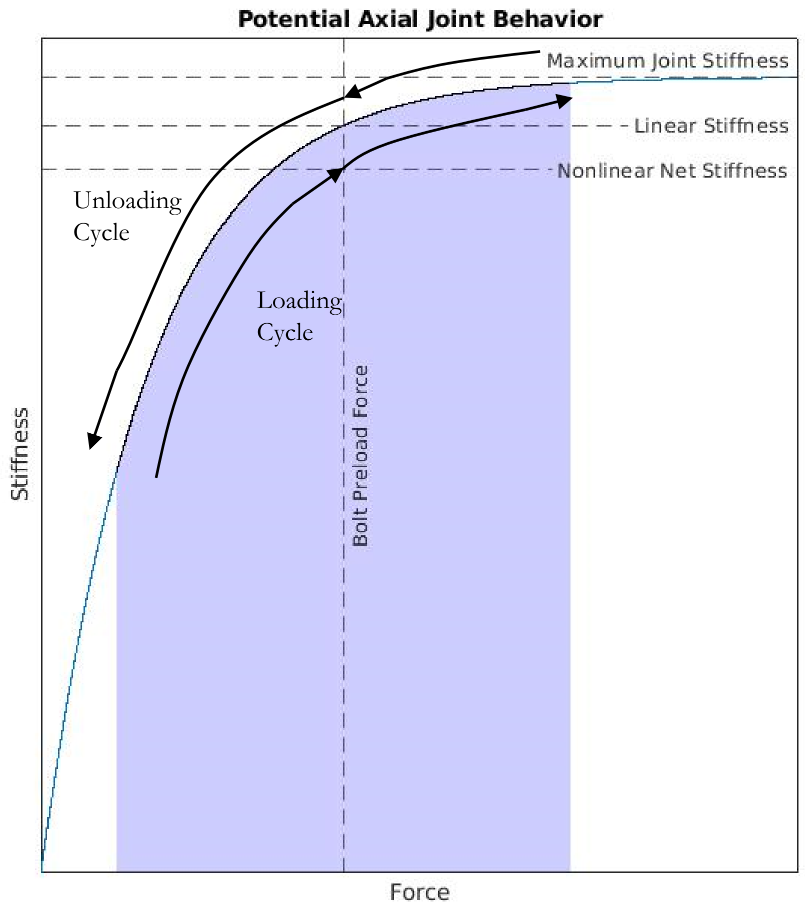

Fig 35. Potential Constitutive Model for Axial Mode

Conclusions and Future Work

Conclusions:

- QSMA can be an effective method for quantifying modal coupling
- Additional research and work will be required to understand how to modally filter data well when there is modal coupling and tightly spaced mode shapes
- Additional research and work will be required in order to effectively model axial modes in joints

Future Work:

- Explore different constitutive models and physical mechanisms
- Explore application of ML to joint modeling
- Mode shape shifting with higher force levels

Appendix

Other Filtration Methods

- **Butterworth**: designed to have a flat frequency response in the passband
- **Chebyshev2**: has a steeper roll-off than the Butterworth filter, but has a stopband ripple (oscillations after the roll-off)
- Both filters were tested on our data; no noticeable difference was observed

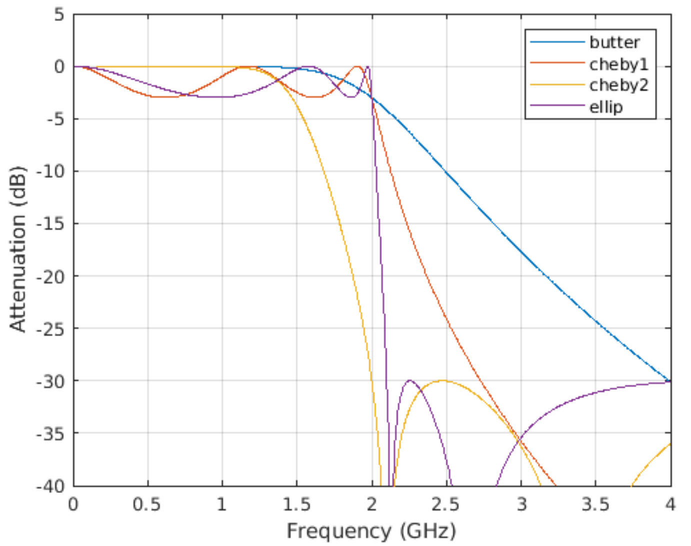

Fig 17a. Roll-off Effects of Different filters

STFT (Short Time Fourier Transform)

- Fourier transform of evenly spaced band pass filters
- Hoped to capture individual modes because we were processing subsets of the data, hence the drop between the bending and axial mode could be targeted
- Nonlinear frequency and damping curves calculated using instantaneous amplitude of FRFs

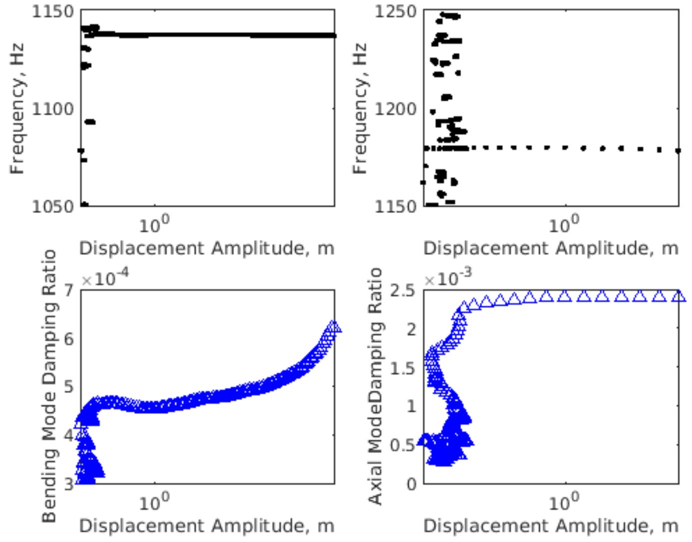

Fig 17b. STFT Frequency and Damping

QSMA: Modal Coupling

- QSMA used on simple bolted structures with weak/negligible modal coupling
  - 2D and 3D bolted cantilever beam models
  - Test hardware for Orion Multipurpose Crew Vehicle
- Modal coupling can be examined by plotting the displacement ratio of each mode vs the peak velocity or the displacement vs the modal amplitude
- Other method of quantifying modal coupling is through an SVD energy based method

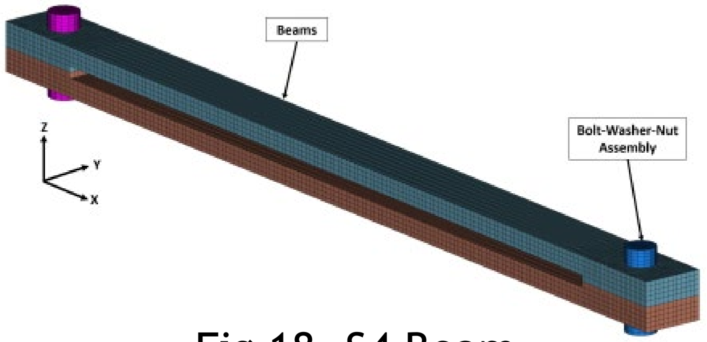

Fig 18. S4 Beam

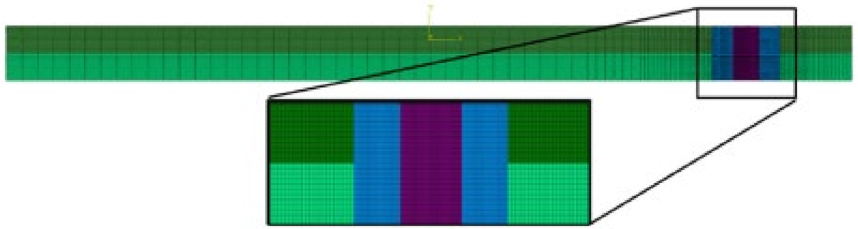

Fig 19. 2D Bolted Cantilever Beam

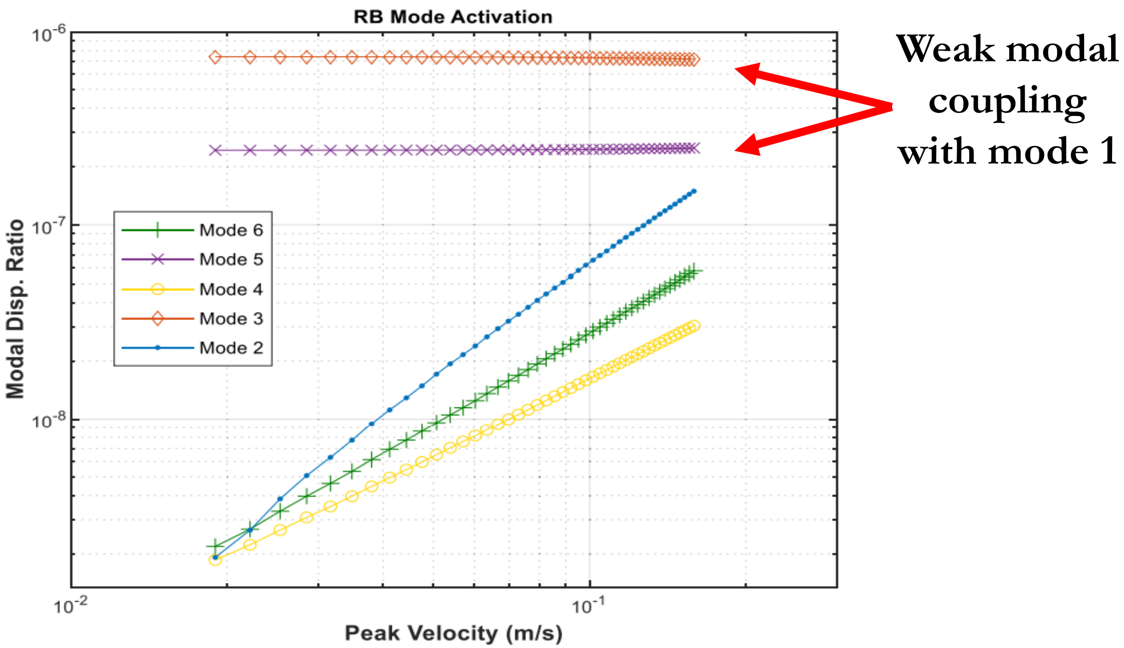

Fig 20. 2D Beam Mode 1 activation

Interface Static Analysis: *Axial Mode*

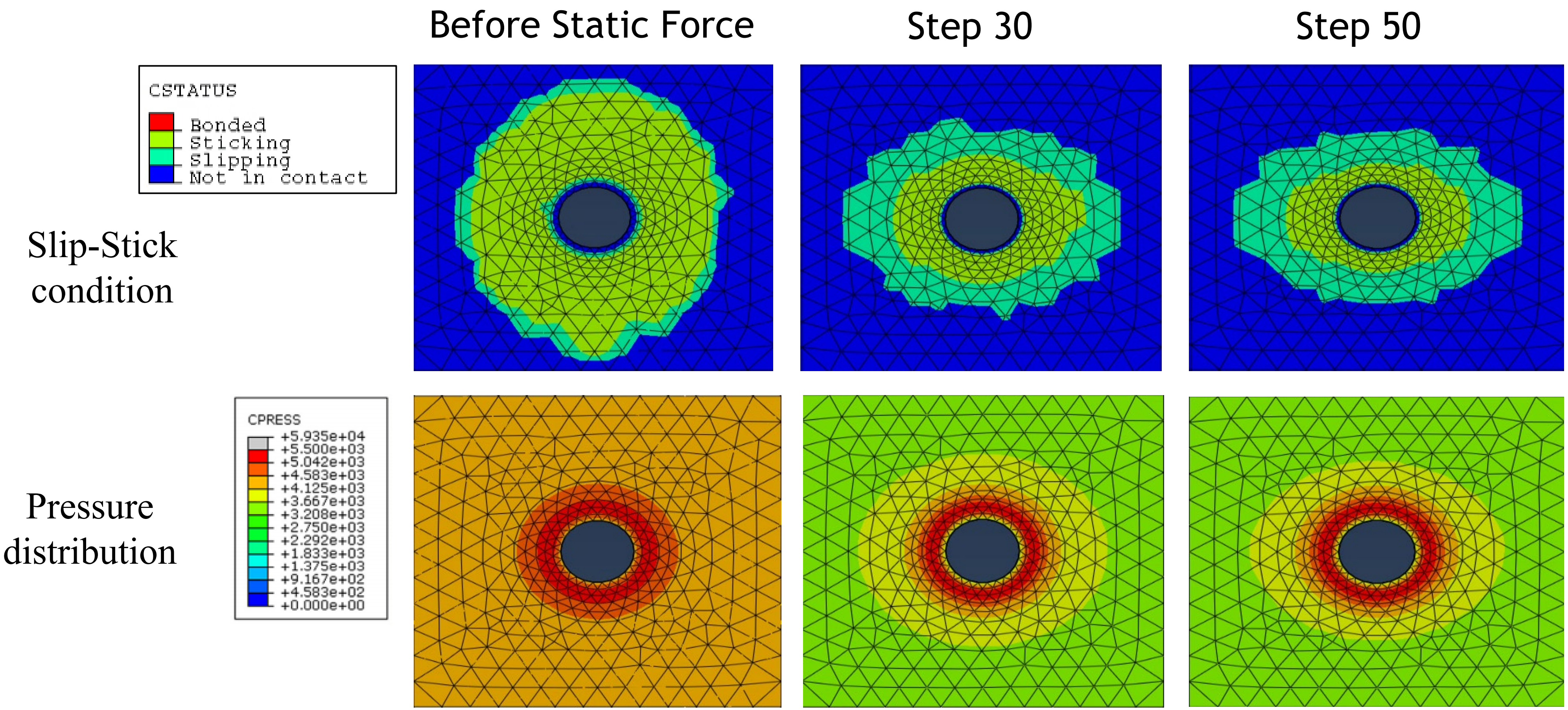

Fig 31a-f. Pressure distribution and Slip-Stick conditions (rep)

- Slipping region is increasing with amplitude while stick region is decreasing
  - This causes decrease of stiffness as amplitude increases (nonlinear softening)
- Pressure magnitude decreasing with amplitude since kettlebell is pulled up from plate

Interface Static Analysis: 2^{nd} *Y bending mode*

Before Static Force | Step 30 | Step 50

Slip-Stick condition

Pressure distribution

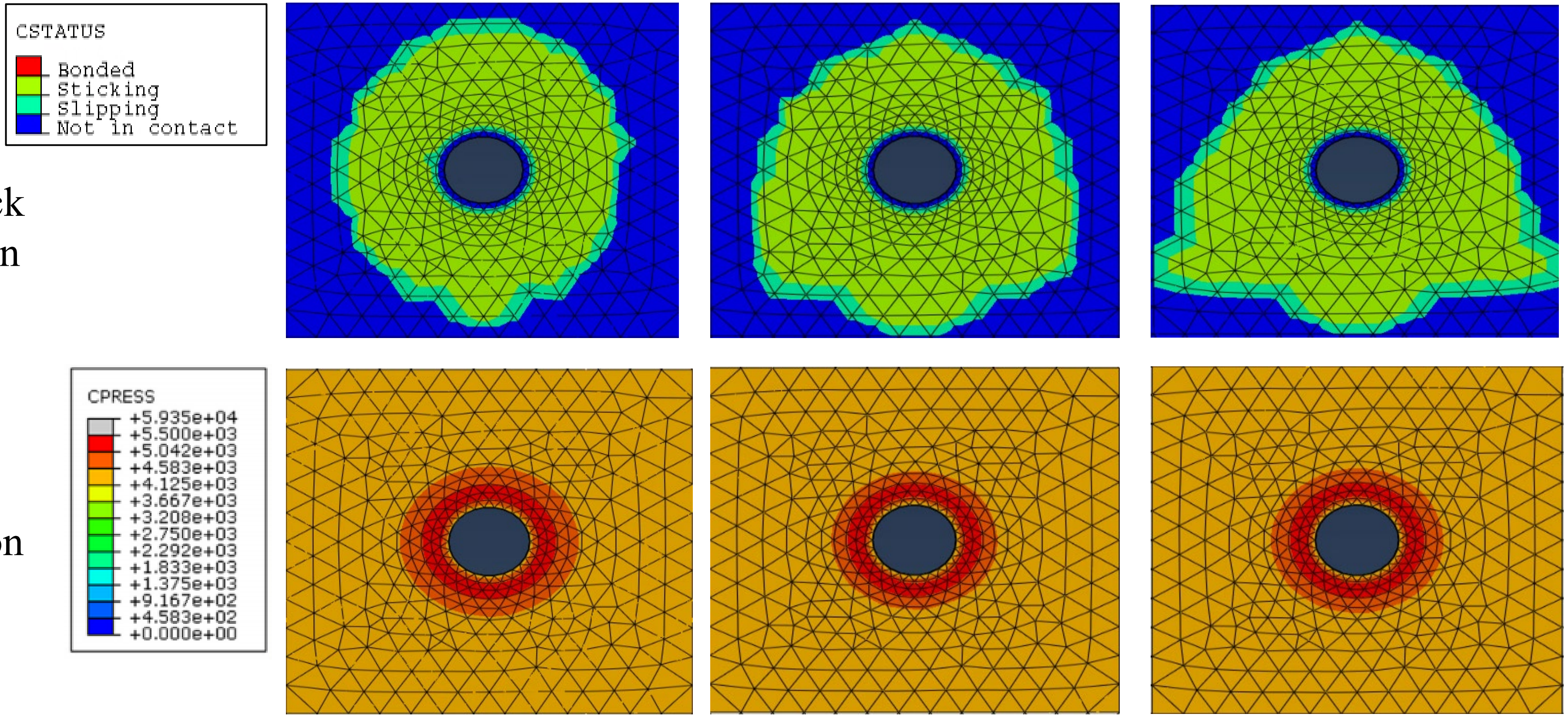

Fig 30a-f. Pressure distribution and Slip-Stick conditions (rep)

- Slipping region remains around edges of stick region while stick region is increasing with amplitude
  - This causes increase of stiffness as amplitude increases (nonlinear hardening)
- Pressure region is increasing with amplitude

Background And Motivation

- Bolted joints are heavily used in simple and complex structures due to the ease of assembly and disassembly.
- They are also a source of nonlinearities and energy dissipation, making a jointed interface difficult to model
  - Dynamics of structure difficult to predict
  - Response can be very different than a monolithic structure with out interfaces
- Main source of nonlinearities occur from the stick-slip behavior of the interface
  - Typically cause nonlinear softening and damping
  - Modal coupling can cause catastrophic failure

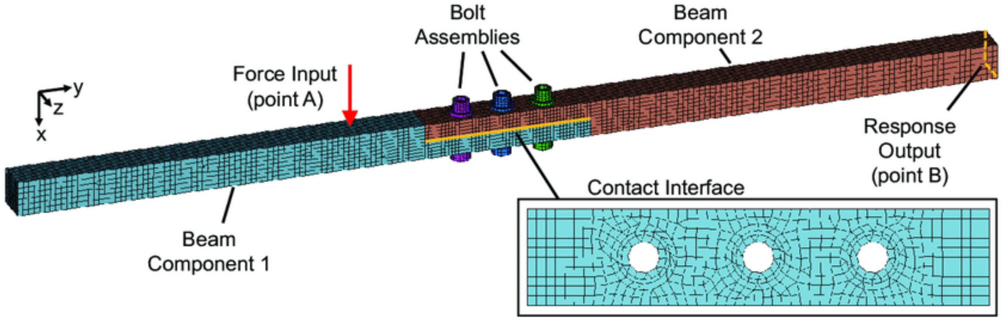

Fig 1. Representative Joint

Fig 2. Large bolted structure

Variation of Nonlinear FEM

- Implements an asymmetric stick region with different frictional properties through out the jointed interfaces
  - Elliptical Stick region allowing finite slip
  - Friction Coefficients: 0.1 and 0.05 for two halves of slip region

Table 3. Adjusted Linear Modes

Mode	*Model*	*Experimental*	*Error*
1st Bending in Z	103.58	101.5	2.05%
1st Bending in Y	168.36	178.9	5.89%
Torsion about X	358.98	348.1	3.13%
2nd Bending in Y	1101.9	1137.3	3.11%
Axial in X	1200.9	1182.3	1.5%
2nd Bending in Z	1486.9	1469.0	1.21%

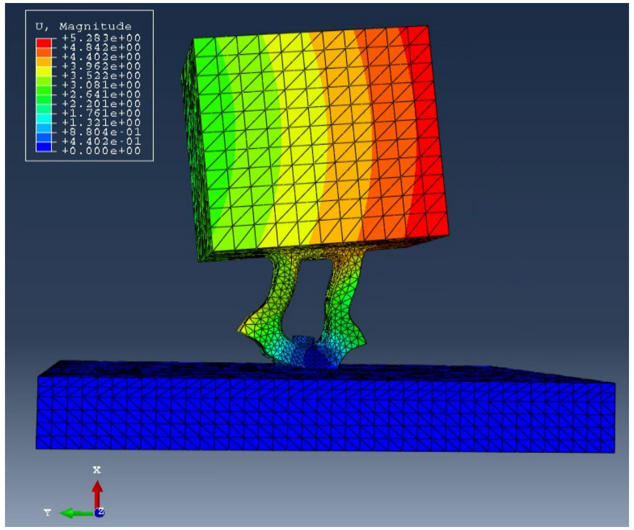

Fig 32. Axial mode with tilt in y-direction

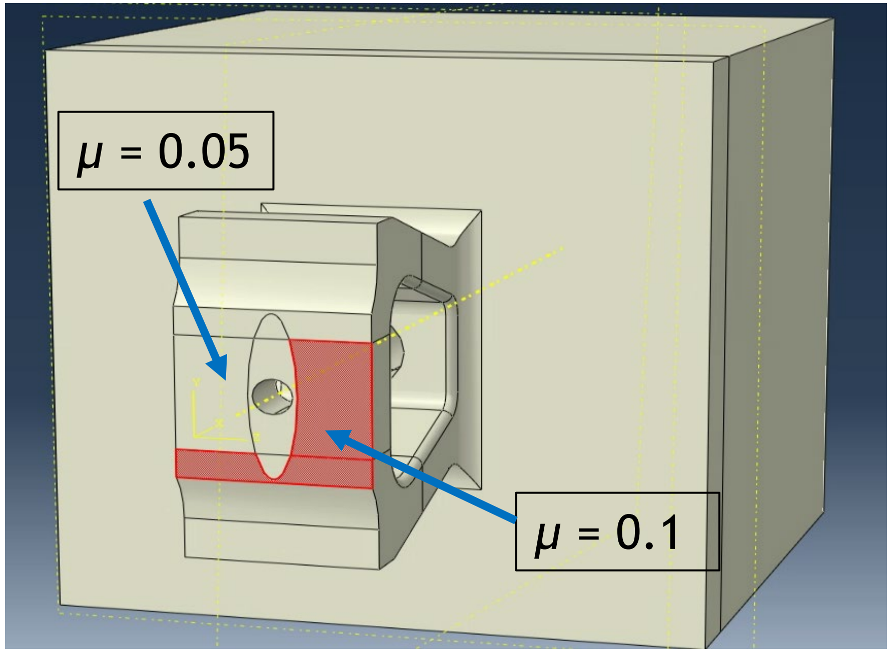

Fig 33. Model joint

The Hurty-Craig-Bampton (HCB) Method

- The Hurty-Craig-Bampton (HCB) method is a dynamic sub-structuring technique which allows the modeler to significantly reduce the size of models
- For an HCB model with 2 super-elements: Size of HCB model = 2*(number of fixed interface modes + 6*boundary nodes)
- MDOF EOM with DOF's partitioned into boundary and interior DOF's

$$\begin{bmatrix} \mathbf{M}_{ii} & \mathbf{M}_{ib} \\ \mathbf{M}_{bi} & \mathbf{M}_{bb} \end{bmatrix} \begin{bmatrix} \ddot{x}_i \\ \ddot{x}_b \end{bmatrix} + \begin{bmatrix} \mathbf{K}_{ii} & \mathbf{K}_{ib} \\ \mathbf{K}_{bi} & \mathbf{K}_{bb} \end{bmatrix} \begin{bmatrix} x_i \\ x_b \end{bmatrix} = \begin{bmatrix} F_i \\ F_b \end{bmatrix}$$

Eqn. 7

- Definition of the HCB transformation

$$\begin{bmatrix} x_i \\ x_b \end{bmatrix} = \begin{bmatrix} \mathbf{\Phi}_{ik} & \mathbf{\Psi}_{ib} \\ \mathbf{0} & \mathbf{I}_{bb} \end{bmatrix} \begin{bmatrix} q_k \\ x_b \end{bmatrix} = \mathbf{\Phi}_{CB} \begin{bmatrix} q_k \\ x_b \end{bmatrix}$$

Eqn. 8

- Applying the HCB transformation and premultiplying by $\mathbf{\Phi}_{CB}^T$ we now define

$$\mathbf{\Phi}_{CB}^T \begin{bmatrix} \mathbf{K}_{ii} & \mathbf{K}_{ib} \\ \mathbf{K}_{bi} & \mathbf{K}_{bb} \end{bmatrix} \mathbf{\Phi}_{CB} = \begin{bmatrix} \omega_k^2 & \mathbf{0} \\ \mathbf{0} & \mathbf{K}_{bb} \end{bmatrix} \qquad \mathbf{\Phi}_{CB}^T \begin{bmatrix} \mathbf{M}_{ii} & \mathbf{M}_{ib} \\ \mathbf{M}_{bi} & \mathbf{M}_{bb} \end{bmatrix} \mathbf{\Phi}_{CB} = \begin{bmatrix} \mathbf{I} & \mathbf{M}_{kb} \\ \mathbf{M}_{bk} & \mathbf{M}_{bb} \end{bmatrix}$$

Eqn. 9

- EOM in HCB space

$$\begin{bmatrix} \mathbf{I} & \mathbf{M}_{kb} \\ \mathbf{M}_{bk} & \mathbf{M}_{bb} \end{bmatrix} \begin{bmatrix} \ddot{q}_k \\ \ddot{x}_b \end{bmatrix} + \begin{bmatrix} 2\zeta_k\omega_k & 0 \\ 0 & 0 \end{bmatrix} \begin{bmatrix} \dot{q}_k \\ \dot{x}_b \end{bmatrix} + \begin{bmatrix} \omega_k^2 & \mathbf{0} \\ \mathbf{0} & \mathbf{K}_{bb} \end{bmatrix} \begin{bmatrix} q_k \\ x_b \end{bmatrix} = \begin{bmatrix} 0 \\ F_b \end{bmatrix}$$

Eqn. 10

Modal Filtering - FRFs

- Influence of the 2nd Bending mode is still present in the FRF for the axial model – there are two peaks
- The increased separation of the bending and axial modes appears to have decreased the peak, but the bending mode is clearly still present
- Other filtering methods must be used to correctly extract the axial mode

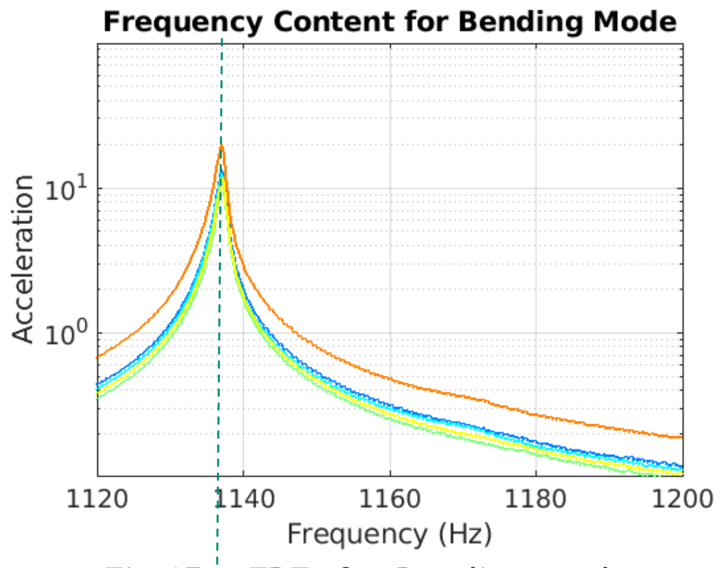

Fig 15a. FRFs for Bending mode

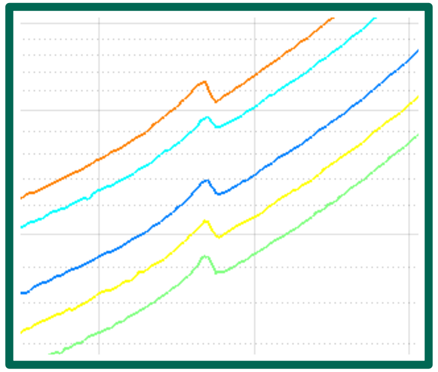

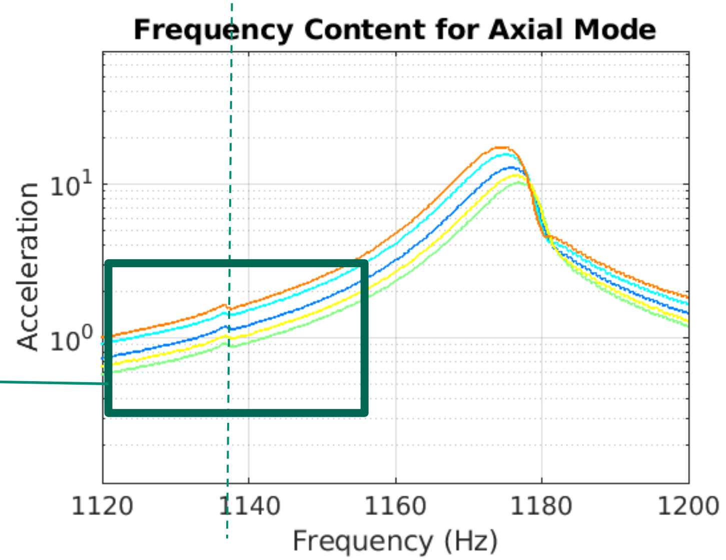

Fig 15b. FRFs for Bending mode

Acknowledgements

This research was conducted at the 2021 Nonlinear Mechanics and Dynamics Research Institute hosted by Sandia National Laboratories and the University of New Mexico.

Sandia National Laboratories is a multimission laboratory managed and operated by National Technology and Engineering Solutions of Sandia, LLC, a wholly owned subsidiary of Honeywell International, Inc., for the U.S. Department of Energy's National Nuclear Security Administration under contract DE-NA-0003525.